Jurnal Kejuruteraan 38(5) 2026: 2435-2455
https://doi.org/10.17576/jkukm-2026-38(5)-27

Plasma Arc Assisted Additive Manufacturing Using Magnesium Alloys: A Review

Walisijiang Tayier[a*] & Shamini Janasekaran[b*]

[a]*Institute of Metallic Materials and Intelligent Manufacturing, School of Metallic Materials and Advanced Manufacturing, Soochow University, Suzhou 215137, China.*

[b]*Center for Advanced Materials and Sustainable Manufacturing, Faculty of Engineering, Built Environment & Information Technology, SEGi University, Petaling Jaya 47810, Selangor, Malaysia*

**Corresponding author: walisitayier@suda.edu.cn, shaminijanasekaran@segi.edu.my*

Received 2 September 2025, Received in revised form 4 February 2026
Accepted 4 March 2026, Available online 30 August 2026

ABSTRACT

Magnesium alloys have emerged as essential materials in biomedical applications due to their biocompatibility and biodegradability. However, the complex geometries and specialized qualities required for sophisticated implants are beyond the reach of traditional manufacturing methods. To overcome these issues, this work explores a novel additive manufacturing (AM) technique called plasma arc-based hybrid heating (arc fusion and laser-based). By leveraging the synergistic effects of plasma and hybrid energy, it enables precise control over extreme processing temperatures, facilitating the fabrication of magnesium alloys with optimized microstructures and enhanced mechanical performance. This research systematically examines the relationship between plasma-driven thermal dynamics, grain refinement mechanisms, and resultant mechanical properties, including tensile strength and fatigue resistance. Furthermore, the study highlights the role of rapid solidification in minimizing defects such as porosity and residual stresses, which are critical factors for implant longevity. These findings underscore the transformative potential of plasma technology in advancing the production of patient-specific biomedical devices, offering a pathway to high-performance, custom-designed magnesium implants. This work not only bridges existing gaps in the additive manufacturing of bio-compatible metals but also establishes a foundation for future innovations in sustainable medical solutions.

Keywords: Plasma; hybrid heating; microstructure; sustainable manufacturing; magnesium alloys

INTRODUCTION

The required operating temperatures have steadily increased across a range of application domains due to technological advancements, particularly in bio-health systems. Based on previous studies, metal-based bio-superalloys have been preferred for these medium- and high-temperature uses. However, these materials are typically constrained to a maximum operational temperature threshold of approximately 600-2000°C, a limit that is becoming progressively inadequate to meet the demands of modern technological requirements (Satya et al. 2020). Metals that possess a melting point under 2000°C are commonly categorized as bio - metals. This group encompasses elements such as Magnesium (Mg), Titanium (Ti), Silver (Ag), Copper (Cu) and Nickel (Ni) (Warlimont & Martienssen, 2020). These metals exhibit a spectrum of bio-compatible characteristics which determine their suitability for health applications, the majority of these metals have a body-centred cubic (BCC) structure. They are typically distinguished by their high or exceptionally high density and excellent wear resistance (Snead et al. 2021). Plasma, an ionized gas with distinct properties from the electromagnetic waves (from microwave), plays a vital role in numerous scientific and industrial areas, including metal additive manufacturing (AM), is an incredibly versatile method for producing parts with complex shapes and highly tailored design elements, especially in small-scale production batches. Moreover, the plasma-based fusion process plays a crucial role in optimizing the buy-to-fly ratio of costly materials and minimizing material waste when compared to traditional subtractive machining processes (Popov et al. 2018). An extensive array of fusion techniques has been devised, employing various energy sources such as microwave, lasers, electron beams, and arcs, along with diverse feedstock forms like wire, sheet, and powder, across a multitude of machine setups (Herzog et al. 2020). Due of their high resolution, flexible processing capabilities, and broad compatibility with a variety of material systems, plasma-based methods presently rule the field of metal joint fabrication, including AM (Schmidt et al. 2022). Plasma-based processes typically utilize micron-scale spherical powders as their primary feedstock. This powder is exist in two different forms, either by (i) depositing a complete layer across the build platform, a method commonly referred to as arc-based powder-bed fusion, or by (ii) directing it specifically to the region of interest via a nozzle, which is generally known as fusion-based directed Energy Deposition (Sahasrabudhe et al. 2020). In both of these processes, a high-energy plasma is employed to selectively solidify the material at specific locations during the fabrication of each metallic layer or intermetallic layer, which typically has a thickness ranging from 20 to 100 micrometers. Although the two processes share common similarities, the primary distinctions are found in the localized plasma spot size, the thickness of each powder layer, the amount of energy input, and the dimensions of the resulting melt pool. These variables result in different temperature gradients, which depend on the particular characteristics of the plasma-based fusion process and the process parameters used. As a result, the material experiences different cooling speeds and thermal gradients (Herzog et al. 2016). Defects are considered as inherent byproducts in fusion melting processes. In the case of powder bed fusion using an arc or beam and directed energy deposition with an electric arc, the prevalent defects encompass porosity, cracking, and elemental contamination. Various forms of porosity may manifest in components fabricated through these techniques. When there is inadequate energy input, porosity may arise due to a lack of fusion between neighboring scan tracks or between successive melting zone. On the other hand, with excessive energy input, porosity can develop as a result of unstable melt pool conditions (DebRoy et al. 2020). When the solidification rate surpasses the time required for the molten metal droplet to spread adequately, issues such as balling and interrupted scan tracks may arise (Sola & Nouri 2019). During plasma fusion process, the formation of fine, spherical pores can occur as a result of the entrapment of atmospheric gases, residual powder particles, or the evaporation of alloying elements (Brennan et al. 2021).

The causes of residual stress can be developed from various sources. One such common source is phase transformation, which may occur in certain materials during the cooling process. Because of the disparity in volume between the several phases, this change may cause stress. Furthermore, different parts of the material experience differing degrees of thermal expansion as a result of localized melting and fast solidification. For materials made by directed energy deposition with an arc beam and powder bed fusion with a laser beam, these stresses are not always troublesome, but they may become so if the residual stress is greater than the material's strength. Problems like warping, delamination, or cracking may occur in these situations (Fang et al. 2020). These cracks and porosities can either lead to the failure of the build or degrade the material's properties. According to welding theory, certain alloys are more prone to liquation cracking or solidification cracking, both of which are types of hot cracking. Solidification cracking happens when a thin film of the remaining liquid is subjected to tensile stresses that exceed the material's crack resistance. Liquation cracking occurs in the partially melted zone next to the fusion line due to the partial melting of the solid. These phenomena can also be observed during certain arc fusion processes (Brennan et al. 2021).

This review aims to be the first comprehensive analysis encompassing bio-compatible metals, especially in Magnesium alloy, as defined above. It is easier to compare the microstructures and characteristics of each biocompatible system made by fusion-based processing by looking at alloying systems in a single evaluation. This method differs from earlier assessments that concentrated on specific biocompatible systems, including magnesium alloy (Mg-based). Moreover, the inclusion of alloy in this review provides a more thorough understanding of the behavior of Magnesium alloy when manufactured using arc fusion process, as known fusion-based additive manufacturing align with SDG 9, Industry, Innovation, and Infrastructure.

MAGNESIUM ALLOYS IN PLASMA (FUSION)-BASED ADDITIVE MANUFACTURING (PBAM)

Additive manufacturing (AM) of magnesium alloys is increasingly gaining interest among the researchers globally, mainly due to its unique design capabilities that surpass those of traditional manufacturing methods, as well as its potential to advance the development of ecological implants. Various processes were employed to demonstrate the additive manufacturing of magnesium, especially focusing on directed energy depositionspecifically plasma or arc additive manufacturing and powder bed fusion (PBF) (Babuska et al. 2021).

POWDER BAD FUSION PROCESSING (PBF)

CAD design, laser or electric processing, also referred to as plasma processing, and numerical control are all used in the Powder Bed Fusion (PBF) manufacturing process to create metallic components with improved qualities. Meanwhile, Figure 1 illustrates the standard Powder Bed Fusion technique, which involves the following steps:

1. Converting a three-dimensional prototype into an STL file, which provides the system with segmented information about the prototype;
2. Applying a thin layer of metal powder to the build container;
3. Based on the prototype information, the system directs a focused laser beam to precisely scan the powder layer. The powder absorbs heat and melts, forming a single layer;
4. The build container then lowers by one layer thickness, and a new powder layer is applied by a roller. The next layer is subsequently created on top of the first layer, and the designed component is gradually formed (Yang et al. 2020).

This advanced manufacturing technique is highly effective for producing complex porous materials and customized implants tailored to meet the specific requirements of individual patients. Over the past two years, several publications have reported on the laser additive manufacturing of magnesium (Mg) scaffolds (Figure 2), which have demonstrated favorable mechanical properties, particularly in terms of tensile modulus, and an acceptable rate of degradation. Specifically, after four weeks of degradation in simulated body fluid, the volume loss of these scaffolds was approximately 20%. Similarly, Kopp et al. (2020) fabricated a WE43 magnesium alloy scaffold using laser additive manufacturing, with pore sizes ranging from 919 µm to 1131 µm. The scaffolds with smaller pores exhibited minimal hydrogen release and only a slight decline in mechanical properties over time. Compared to other methods for producing porous structures, laser additive manufacturing offers precise control over the architecture of the scaffold. The integration of computer-aided design CAD) and computed tomography (CT) technologies enables the seamless customization of bone implants for specific patients and various anatomical defect sites.

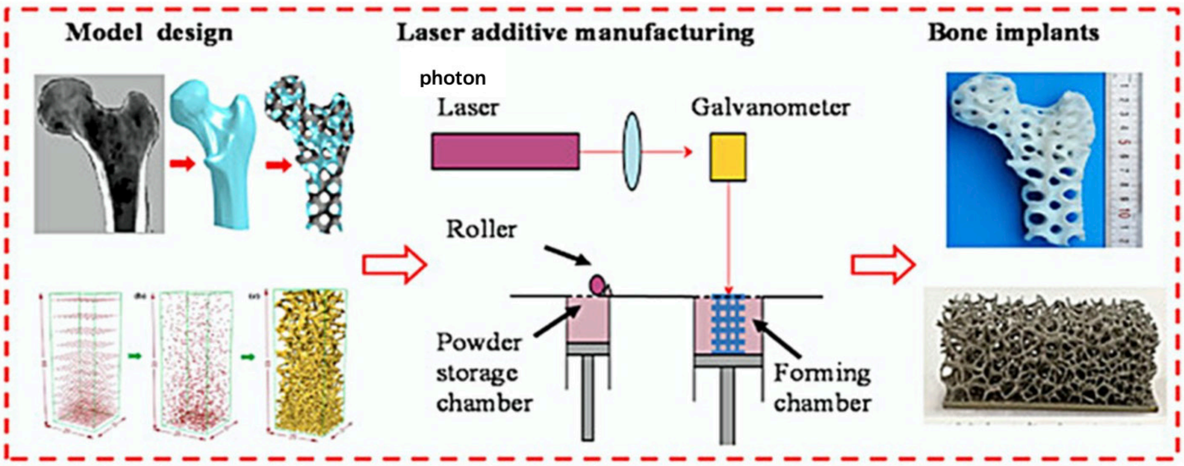

FIGURE 1. Bone implant manufacturing utilizing a cownventional powder bed fusion technique based on the principles of photon based additive manufacturing (Yang et al. 2020)

Fusion based additive manufacturing involves rapid melting and solidification processes, which significantly refine the microstructure of materials. In their investigation of the microstructural evolution of WE43 magnesium alloy during fusion-based AM, Florian Bär et al. showed that localized heat distribution inside the molten pool influences the final microstructure. Interestingly, the grain size of WE43 made using fusion-based AM was significantly lower than that generated using traditional casting techniques, as seen in Figure 3. This phenomenon is attributed to the rapid cooling rates inherent to fusion based AM, which effectively interrupt grain growth and result in a fine-grained microstructure. Fine-grain strengthening, a mechanism that enhances the mechanical properties of magnesium components by reducing grain size, is thus facilitated by fusion-based AM. The grain size also exerts a significant influence on the corrosion behavior of magnesium alloys, although the underlying mechanisms remain a subject of debate. Some studies have proposed that grain boundaries act as barriers to corrosion, thereby hindering the corrosion kinetics (Ralston & Birbilis 2019; Jiang et al. 2021). On the contrary, other researchers have suggested that grain boundaries may introduce crystallographic defects that accelerate the corrosion process (Zhang et al. 2021). The contradictory findings highlight the need to consider the specific alloy type and the range of grain sizes under investigation. For instance, ZK60 magnesium alloy with refined grains, as reported by (Shuai et al. 2022), exhibited enhanced mechanical properties and a reduced corrosion rate, supporting the hypothesis that grain boundaries can function as corrosion barriers.

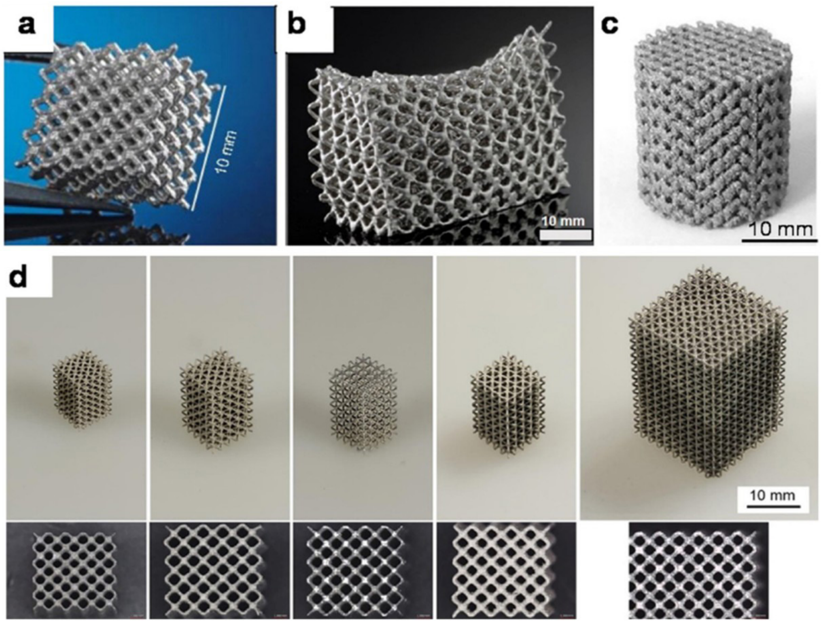

FIGURE 2. WE43 scaffolds featuring diverse structural designs were fabricated through a photon based additive manufacturing process (Qin et al. 2020)

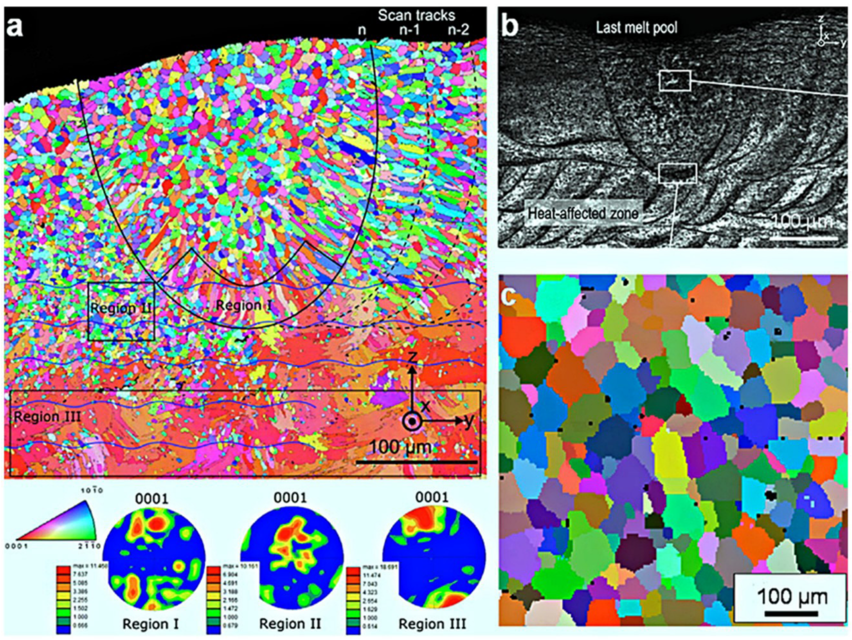

FIGURE 3. (a) Microstructure of additively manufactured WE43, as revealed by Backscattered Kikuchi Diffraction (BKD) mapping; the color scheme illustrates the orientation of hexagonal Mg grains relative to the z-direction, (b)Corresponding scanning electron microscopy (SEM) image of the cross-sectional last scan track of as-built WE43, (c)Electron backscatter diffraction (EBSD)map of the microstructure of cast WE43, exhibiting relatively coarse grains (Zhang et al. 2021).

PLASMA ARC ADDITIVE MANUFACTURING PROCESS

Plasma arc additive manufacturing, a process categorized under directed energy deposition (DED) within the broader realm of (AM), was employed for the fabrication of magnesium-based biomedical implants. This technique mitigates the formation of dendritic structures, which are often observed during the AM of magnesium alloys. The resultant microstructure is characterized by refined grains and minimized defects, thereby enhancing the material's mechanical integrity. Specifically, the plasticity and fatigue properties of additive fabricated components are significantly improved due to the coarse microstructure that develops during the process (Madhuri et al. 2021). The macrostructure, microstructure, and tensile properties of additive produced AZ31 magnesium alloy samples are influenced by the pulse frequency. As the pulse frequency increases, weld pool oscillations become more pronounced, and the cooling rate decreases, leading to a reduction in grain size. Specimens fabricated at pulse frequencies of 5 Hz and 10 Hz exhibit finer equiaxed grains (21 μm), higher ultimate tensile strength (260 MPa), and greater yield strength (102 MPa) compared to conventionally forged AZ31 alloy (Guo, et al., 2021). Increased deposition feed rates and speeds promote the formation of finer grain structures. In addition to these parameters, another technique utilized in the (AM) of magnesium (Mg) implants is paste extrusion deposition (PED), which is classified under material extrusion processes. This method offers unique advantages, such as the potential to develop magnetic implants for drug delivery and the ability to incorporate hydroxyapatite and collagen into Mg implants. These features enhance the biomimetic properties of the implants, closely replicating the composition and functionality of natural bone (Karunakaran et al. 2020). Elevated tool forces and deposition speeds result in higher cladding temperatures, which in turn produce components with increased porosity. This process also enhances the mechanical properties of the components, including strength and ductility. Furthermore, substantial residual stresses are introduced into the material by greater thermal gradients across the workpiece cross-section. The compressive and tensile strengths of magnesium implants made from MgP alloy utilizing binder jetting procedures are on par with those of natural bone. Choosing a binder agent is essential since; in order to avoid negative reactions, it must be chemically inert regarding the powder. Given magnesium's combustibility and limited thermal stability, additive manufacturing technologies like binder jetting are essential to produce Mg-based implants (Gunathilake et al. 2021). A schematic overview of various additive manufacturing processes used in the fabrication of magnesium components is presented in Figure 4.

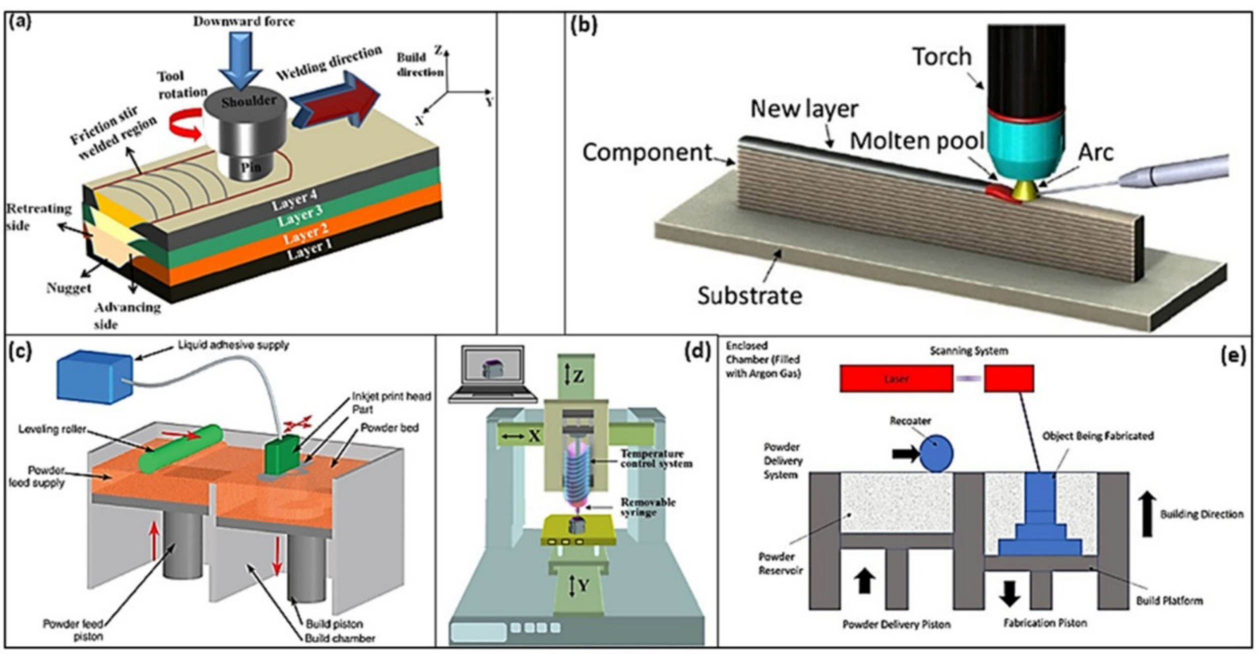

FIGURE 4. Schematic illustrations comparison of (a) Friction Stir Additive Manufacturing (FSAM), (b) Plasma Based-Wire Arc Additive Manufacturing (WAAM), (c) Binder Jetting, (d) Paste Extrusion Deposition (PED),and (e) Selective Laser Melting (SLM) (Palanivel et al. 2023; Rodrigues et al. 2020; Moritz & Maleksaeedi 2021; Jiao et al. 2022).

The qualitative attributes and mechanical properties of specimens produced via additive manufacturing were found to surpass those of primary components and samples fabricated using conventional die-casting and hot extrusion techniques, as reported by researchers. Palanivel (Palanivel et al. 2020) demonstrated that specific welding parameters in solid state additive manufacturing resulted in Mg-4Y–3Nd alloy specimens with enhanced surface quality. In the "as-fabricated" condition, the maximum hardness reached 115 HV, which increased to 135 HV after aging. Compared to the base material, welding characteristics improved strength by up to 400 MPa and enhanced ductility by 17%. Wei (Bose et al. 2023) observed that selective laser melting, a powder bed fusion process, produced magnesium alloy AZ91D specimens with great microhardness and tensile strength relative to die-cast magnesium counterparts. Besides, Yook et. al. (2019) found that orientation, printing angle, and raster angle had negligible effects on the fatigue strength of 3D-printed Mg alloys. Additionally, heat treatment was shown to reduce porosity and enhance fatigue resistance.

WIRE ARC ADDITIVE MANUFACTURING PROCESS

MORPHOLOGY

A developing technique that overcomes magnesium alloys' weak plastic deformation ability is wire arc additive manufacturing, or WAAM. In WAAM, the wire is melted by the heat of an arc and deposited layer by layer onto a substrate, constructing components from the bottom up (Horgar et al. 2020) (Chen et al. 2021). Compared to other AM techniques, WAAM offers higher production efficiency, making it ideal for fabricating large, low-complexity parts without the constraints of a build platform. Furthermore, WAAM achieves a deposition rate of 3–7.8 kg/h per arc, significantly exceeding the 0.12–0.6 kg/h rate of single-laser or electron beam methods, with further increases possible using multiple arcs (Mazumder, Dutta, Kikuchi, & Ghosh, 2020). Its energy efficiency typically exceeds 70%, far surpassing selective laser melting (SLM) (2%–5%) and electron beam melting (EBM) (15%–20%) (Shi et al. 2020) (Li et al. 2023) (Janasekaran & Mann 2020). Additionally, WAAM claims nearly 100% material utilization, and its large, long-lasting molten pool allows bubbles ample time to escape (Cho et al. 2022) (Jia et al. 2020). These systems can integrate various sensors to monitor interlayer temperature, weld signals, weld channel geometry, and metal transfer behavior, which enables precise process control and enhanced production quality (Xiong et al. 2021) (Denlinger et al. 2020). The equipment is relatively simple, facilitating rapid industrialization. Significant heat accumulation results from WAAM's larger molten pool and slower heat dissipation as the number of deposited layers rises. This causes the metal to solidify more slowly, which can lead to poor part quality and irregular surface morphology. As a result, post-processing machining is frequently required to satisfy specifications for surface smoothness and dimensions.

To optimize surface morphology, researchers modified relevant process parameters to enhance the surface functionality. For example, Guo et al. (2021) studied the effects of pulse frequency on AZ31 magnesium alloy parts fabricated using gas tungsten arc welding (GTAW). They found that higher pulse frequencies improved surface smoothness but also increased molten pool turbulence, causing resonance effects and inconsistent sample widths (Figure 5). Similarly, Wang et al. (2020 – study on the deposition accuracy of omni-directional GTAW-based additive manufacturing) developed a wire melting model to assess the influence of wire feed speed. All the results from their studies revealed that speeds between 0.35–0.40 m/min led to process instability, discontinuous weld seams, and significant dimensional deviations from the intended geometry. Thus, this speed range should be avoided to ensure consistent part quality. Regarding shielding gas applications, blended gas mixtures demonstrate superior performance compared to pure single-component gases. Optimal protection is achieved through combinations of argon with helium, or carbon dioxide with hydrogen additions. The chosen shielding methodology also significantly influences component surface characteristics. Researchers led by Ding (Ding et al. 2019) developed an innovative localized shielding apparatus for WAAM applications (illustrated in Figure 6b). This innovative design, which has uniform gas distribution at the entrance and vertically oriented outlet flow, uses laminar flow principles to generate a carefully controlled local shielding environment. According to experimental results, this sophisticated shielding system maintains atmospheric contamination below 2000 parts per million at a standoff distance of 30 mm, which is an improvement factor of more than 1000× over traditional shielding designs (Figure 6a). Technological advancement substantially enhances both part protection during deposition and final product quality. To achieve superior surface finish in AM, researchers have integrated machining operations with the WAAM process. When using interlayer milling, Zhang's team's (Zhang et al. 2020) experimental investigations showed a substantial association between dimensional precision and machining parameters. According to their research, the best results are obtained when the machining depth is kept between 0.4 and 1.2 mm, which results in a

22.9% increase in surface smoothness and a 31.6% decrease in the amount of finishing material needed. However, increasing the cut depth to 1.6 mm produces adverse effects, with surface irregularities and material waste exceeding conventional WAAM results by 71.5% and 22.5% respectively. The underlying mechanics were examined through fluid dynamics analysis (Figure 9). In standard WAAM operations, molten material exhibits rapid downward flow along deposition surfaces, resulting in suboptimal solidification angles (θ), compared to hybrid processing methods (Figure 7a). These acute angles directly correlate with diminished surface quality. The hybrid approach promotes outward material flow and surface redistribution (Tayier et al. 2023). At optimal machining depths (<1.2 mm), the retained curved edge profile facilitates proper melt behavior when combined with appropriate processing speeds (Vsp), enabling near-ideal solidification angles approaching π (Figure 7b). Excessive machining depths (>1.2 mm) create nearly full cross-section cuts, prolonging lateral material diffusion and inducing undesirable profile variations along sidewalls (Figure 7c), ultimately degrading surface characteristics.

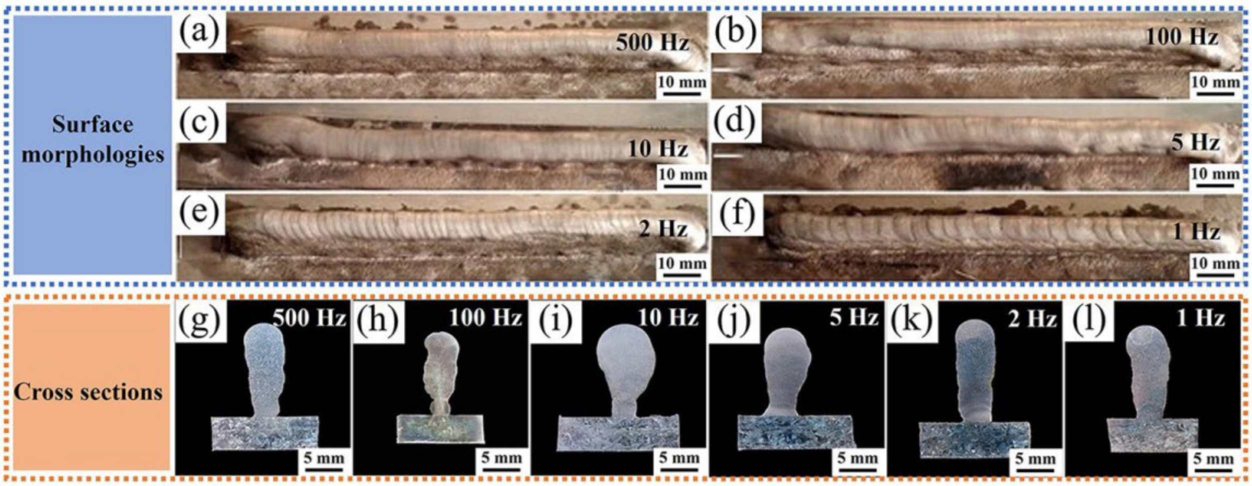

FIGURE 5. Surface morphologies and cross sections of the GTAW fabricated AZ31 magnesium alloy parts with different pulse frequencies: a and g 500 Hz; b and h 100 Hz; c and i 10 Hz; d and j 5 Hz; e and k 2 Hz; f and l 1 Hz (Guo et al. 2021)

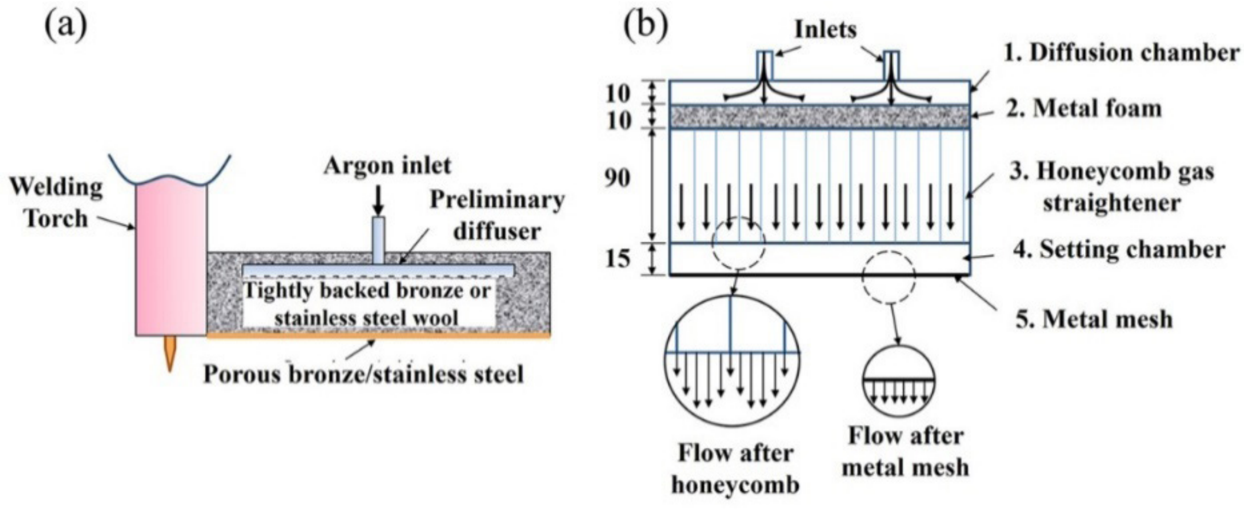

FIGURE 6. Schematic diagram of shielding device: a conventional local shielding device; b laminar flow local shielding device design (Ding et al. 2019)

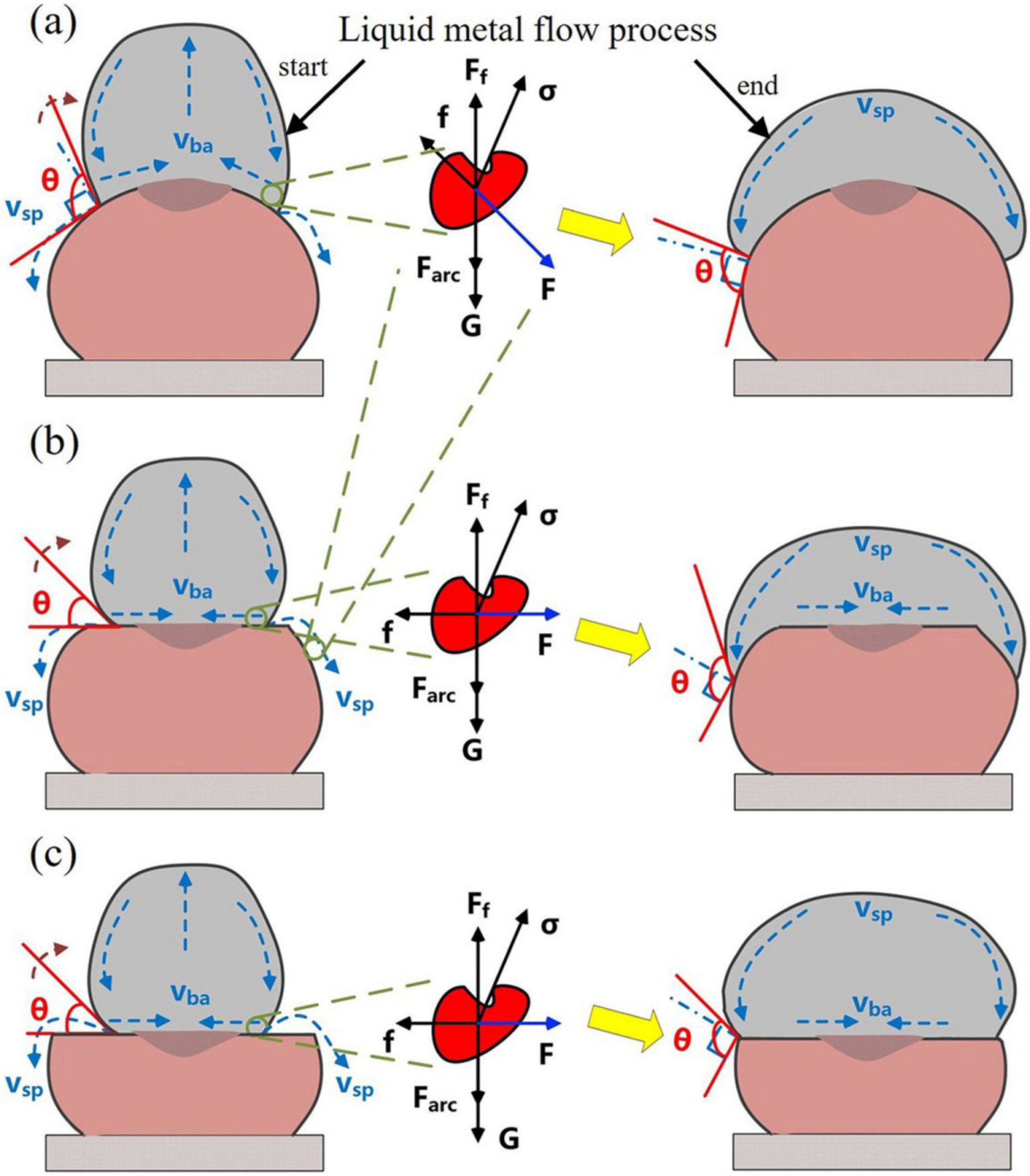

FIGURE 7. Schematic diagram of the forces on liquid metal for different processes: a WAAM; b mixed manufacturing (t is less than1.2 mm); c mixed manufacturing (t is greater than 1.2 mm). Where σ is surface tension, θ is liquid–solid contact angle, G is gravity, t is the milling thickness, Ff is buoyancy, f is friction, Farc is arc force and F is the resultant (Zhang et al. 2020)

POROSITY

Porosity formation represents a significant quality challenge in WAAM-produced components, unfavorably affecting their mechanical performance and structural integrity (Edwards, O'conner, & Ramulu, 2022). This phenomenon primarily stems from hydrogen's temperature-dependent solubility characteristics in magnesium alloys (Li et al. 2020). During solidification, dissolved gases accumulate at the advancing solid-liquid boundary, eventually nucleating into voids as molecular clusters. The relatively high solidification rates characteristic of WAAM processes limit gas bubble migration and escape from the melt pool. One can classify the underlying causes of porosity as either process-induced or material-related. The quality of the feedstock is crucial from a materials standpoint since the wire and substrate materials frequently have surface impurities such as leftover lubricants, adsorbed water vapor, and different organic compounds. During deposition, these contaminants may introduce gas-forming substances into the molten metal. Nevertheless, rigorous material preparation and handling procedures are essential for porosity mitigation.

Process-induced porosity in WAAM components often exhibits irregular morphology, particularly when resulting from suboptimal deposition strategies or inconsistent process parameters. Complex toolpaths or variable deposition conditions frequently leads to incomplete fusion or material expulsion, creating void formations within the fabricated structure. Researchers conducted detailed porosity characterization using advanced imaging techniques on GTAW-produced AZ31 magnesium alloy specimens (Fang et al. 2022). X-ray computed tomography (XCT) analysis revealed distinct pore distributions between upper and lower sections of the test walls (illustrated in Figure 8). Quantitative evaluation showed 358 voids in upper regions compared to 453 in lower sections (Figures 11a-b), with both areas demonstrating comparable void fractions averaging approximately 0.01%. In both zones, these cavities' dimensional properties exhibited patterns of normal distribution. Both the top and lower sections' void dimensions, according to microstructural analysis, showed normal distribution patterns, with a peak frequency at around 68 μm (Figure 8c).Geometric characterization of these cavities demonstrated predominantly ellipsoidal morphologies, with sphericity values concentrated between 0.4-0.8 (Figure 8d). Complementary research by Klein et al. (2022) involving SEM examination of CMT-fabricated AZ61A tensile specimens confirmed the presence of gas-induced voids on fracture surfaces.

Effective porosity mitigation requires a multi-faceted approach: First, maintaining scrupulous cleanliness of both feedstock materials and substrate surfaces is essential. Second, employing premium-grade shielding gases minimizes atmospheric contamination. Third, precise thermal management during deposition helps prevent void formation. Additionally, supplementary techniques like interlayer mechanical compression can further enhance material density.

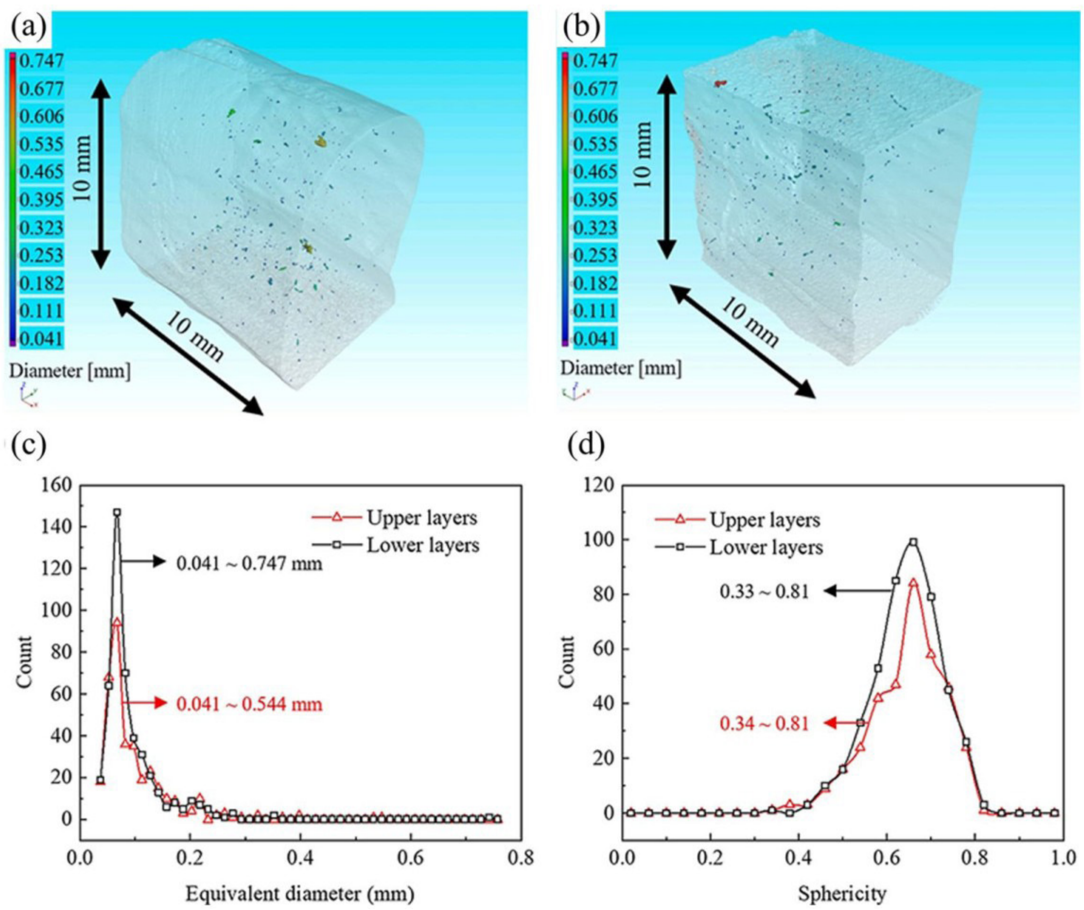

FIGURE 8. 1 XCT reconstructed volume of the a top and b bottom layers, as well as c equivalent diameter and d sphericity of the defect distribution (Fang, et al. 2022)

CRACKS

Thermal-induced cracking in WAAM components stems from both process thermal dynamics and material characteristics (Wu, et al., 2020). These fractures typically manifest as either solidification-related or intergranular types. Solidification cracking occurs when material solidification behavior is compromised, often due to restricted molten metal flow or excessive strain during cooling. Intergranular fractures primarily result from microstructural variations at grain boundaries, including precipitate formation or dissolution effects (Yue et al. 2020).

Microstructural investigations of WAAM-produced AZ80M components revealed defect-free interfaces with substrates, though limited cracking was observed at certain boundaries (Guo et al. 2020). By analysing tensile specimens, similar investigations on Mg-3.2Y-1.6Nd-0.5Zr alloy deposits revealed fracture mechanisms (Figure 9). Examining the area around fracture surfaces showed noticeable cracking [Figures 9 (a-b)], which was caused by brittle Mg24Y5 intermetallic phases at grain boundaries. Figure 9d illustrates crack propagation along grain boundaries, significantly reducing material ductility. The mechanical incompatibility between brittle secondary phases and the α-Mg matrix creates localized stress concentrations. As deformation accumulates beyond critical thresholds, brittle phase fracture initiates micro voids, ultimately causing catastrophic failure and diminished elongation (Eivani et al. 2021).

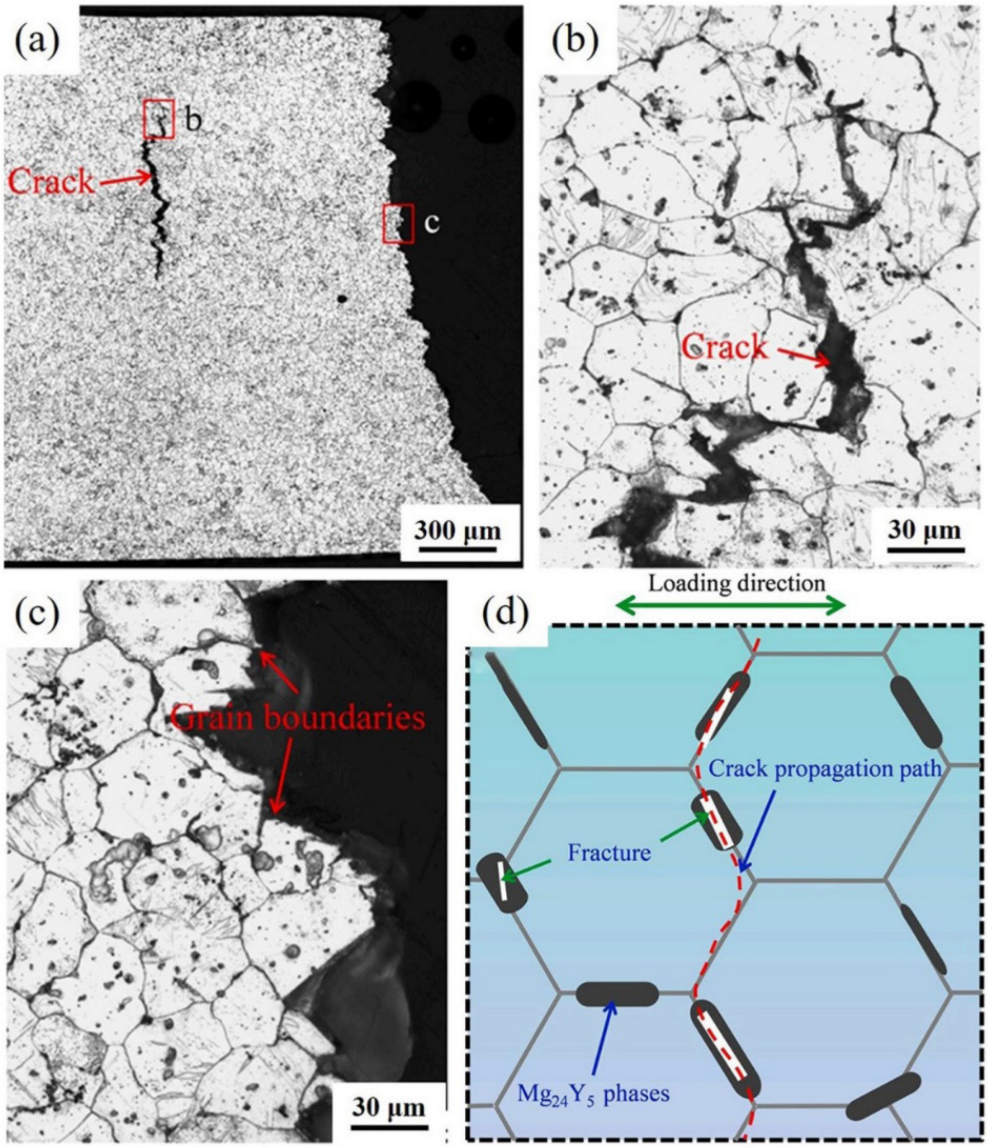

FIGURE 9. Side views of fracture surfaces of WAAM tensile samples: a WAAM samples; b and c the details in a; d schematic diagram of the WAAM fracture 9 (Guo et al. 2020)

INDUCTION HEAT ASSISTED AM

Additive manufacturing (AM) systems utilize various energy delivery mechanisms to facilitate layer-by-layer material deposition. These mechanisms fundamentally differ in their energy transfer methodology, being categorized as either direct-contact or remote energy application systems (Taminger & Hafley 2023). Direct-contact systems, commonly employed in extrusion-based AM, feature heating elements physically attached to or surrounding the extrusion apparatus (Akhoundi et al. 2020). This configuration relies on resistive heating principles, where electrical current passing through conductive coils generates thermal energy (Turner & Gold 2021). Such direct-contact heating proves particularly effective for polymer processing in AM, where relatively modest temperatures suffice. Nevertheless, resistive heating is less appropriate for metal AM applications due to unique thermal problems. Significant thermal inertia and energy losses are introduced by the sequential heat transfer pathway, which goes from the heating element to the extruder to the metal feedstock. Achieving sufficient temperatures for metal fusion necessitates oversized heating elements with substantial power requirements, adversely affecting system portability and operational efficiency. These limitations become particularly problematic given metal AM's demand for rapid thermal cycling and precise temperature modulation. Subsequently, remote energy delivery systems have emerged as the preferred solution for metal additive processes. Induction heating represents one such non-contact approach, offering rapid metallic feedstock heating capabilities. Its economical implementation and straightforward architecture position it favorably among alternative non-contact energy sources (Semiatin 2000).

1. The fundamental architecture of an induction heating apparatus comprises three primary subsystems:operator control interface
2. high-frequency power converter
3. electromagnetic coil assembly (illustrated in Figure 10).

The control interface enables real-time process monitoring and parameter adjustment based on operational demands. Thermal distribution characteristics in the target material are principally determined by the coil configuration and its spatial constraints. The power conversion unit generates precisely regulated alternating currents at specified frequencies to establish the necessary electromagnetic flux around the work coil (Vishnuram et al. 2021). Eddy current production and magnetic hysteresis effects are two different physical principles that underlie induction heating. A time-varying electromagnetic field is produced by the system's power converter, which supplies the coil with high-frequency alternating current (usually 20–200 kHz). When conductive materials are positioned within this field, circulating currents form on the material surface (demonstrated in Figure 11). These localized current loops induce molecular agitation within the metallic structure, with electron flow resistance converting electrical energy into thermal energy.

For ferromagnetic materials, additional heating occurs through magnetic domain realignment. Magnetic dipoles are constantly reoriented by the oscillating magnetic field, and energy losses during this process show up as heat. As temperatures rise toward the Curie point, where materials lose their ferromagnetic characteristics and the hysteresis effect stops, this phenomenon becomes less noticeable (Rudnev et al. 2011). The electromagnetic coil serves as the critical energy coupling component in induction heating systems, facilitating power transfer to the target material. Typically fabricated from high-purity copper, these coils leverage the metal's exceptional electrical and thermal properties - notably its minimal resistance to current flow and superior heat dissipation capability compared to alternative conductive alloys. These characteristics enable rapid thermal energy transmission, making copper the preferred choice for high-performance induction applications. Coil configuration significantly influences several thermal parameters including heating velocity, thermal distribution profile, and energy penetration characteristics (Figure 12 demonstrates these geometric dependencies). The depth of thermal energy deposition is particularly affected by the electromagnetic skin effect - a phenomenon where alternating current tends to concentrate near the conductor surface. This skin depth (δ) is mathematically determined by the operational frequency, material resistivity, and magnetic permeability of the heated component, as expressed by the relation in Equation 1:

$$d = 503\sqrt{\frac{\rho}{f.\mu_r}} \tag{1}$$

The mathematical expression incorporates three key parameters: ρ represents the material's specific electrical resistance, ω denotes the angular frequency of the alternating current (where $\omega = 2\pi f$), and μ indicates the material's magnetic permeability relative to free space (Smalcerz & Przylucki, 2023).

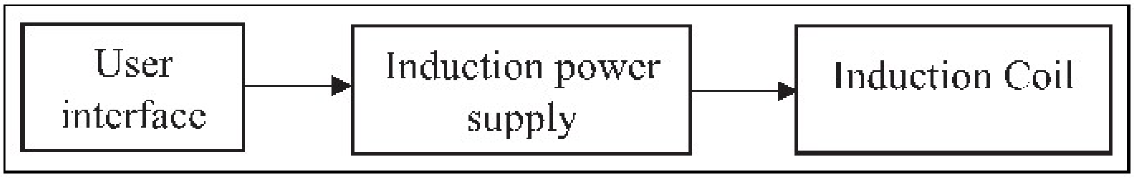

FIGURE 10. Block diagram of the induction heating system

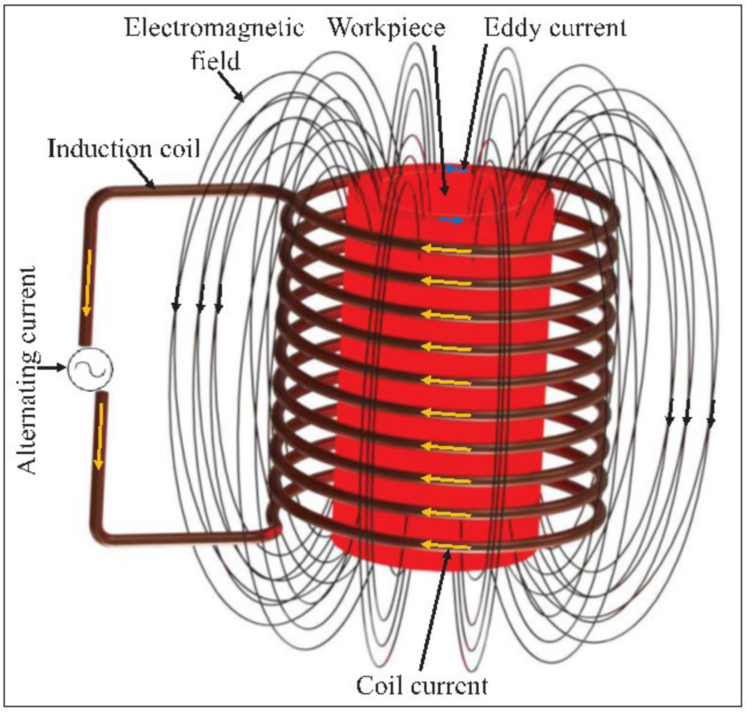

FIGURE 11. Typical induction heating principle (Rudnev et al. 2011)

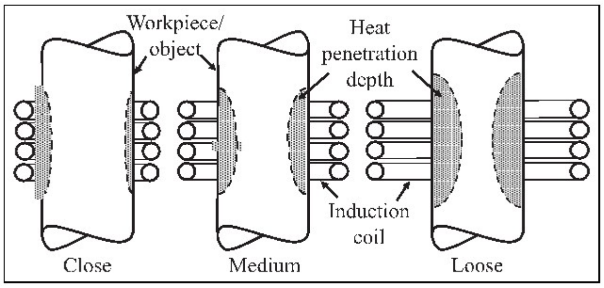

FIGURE12. Heat penetration depth in workpiece (Rudnev et al. 2011).

ELECTRON BEAM AM

Advanced manufacturing techniques enable unprecedented design freedom for engineering components, particularly for lattice-based architectures that achieve significant weight reduction. Electron beam technology generates sufficient thermal energy to fuse various metallic materials, ranging from aluminum-based alloys to specialized cobalt-chromium superalloys. Magnesium alloys are currently the subject of a lot of research because of their remarkable strength-to-weight ratios, biological compatibility, and environmental resilience, which make them perfect for medical applications (Price et al. 2023).

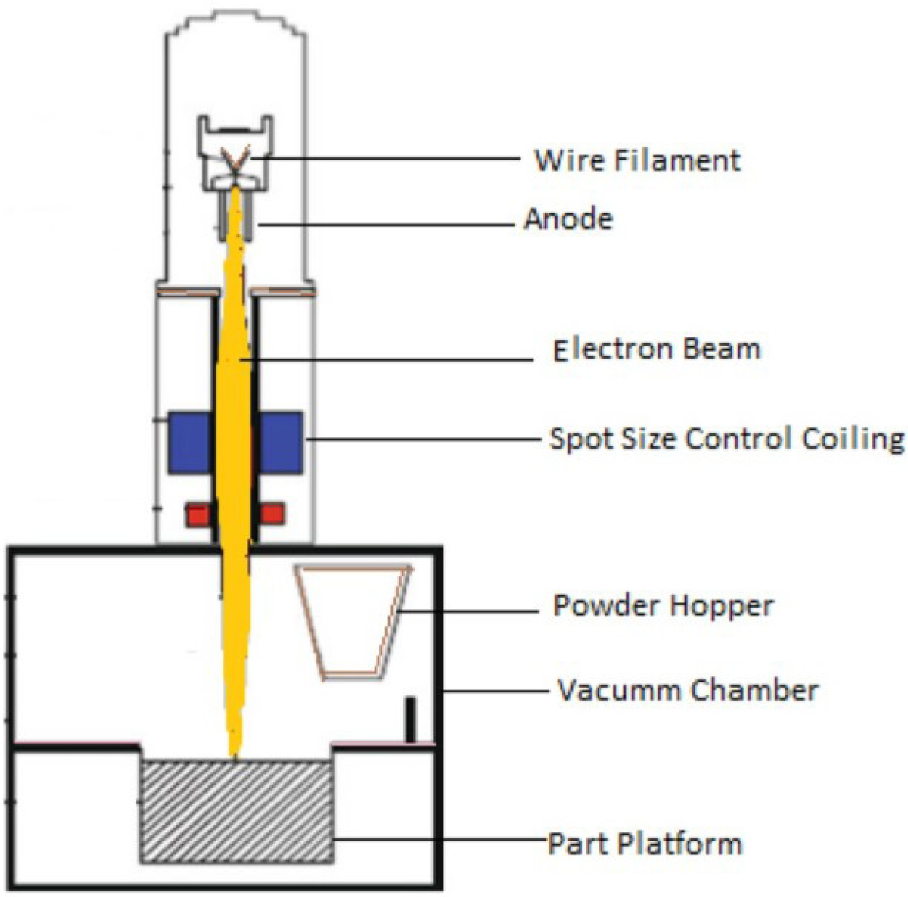

FIGURE 13. Electron beam melting technology (EBT) (Schwerdtfeger et al. 2020)

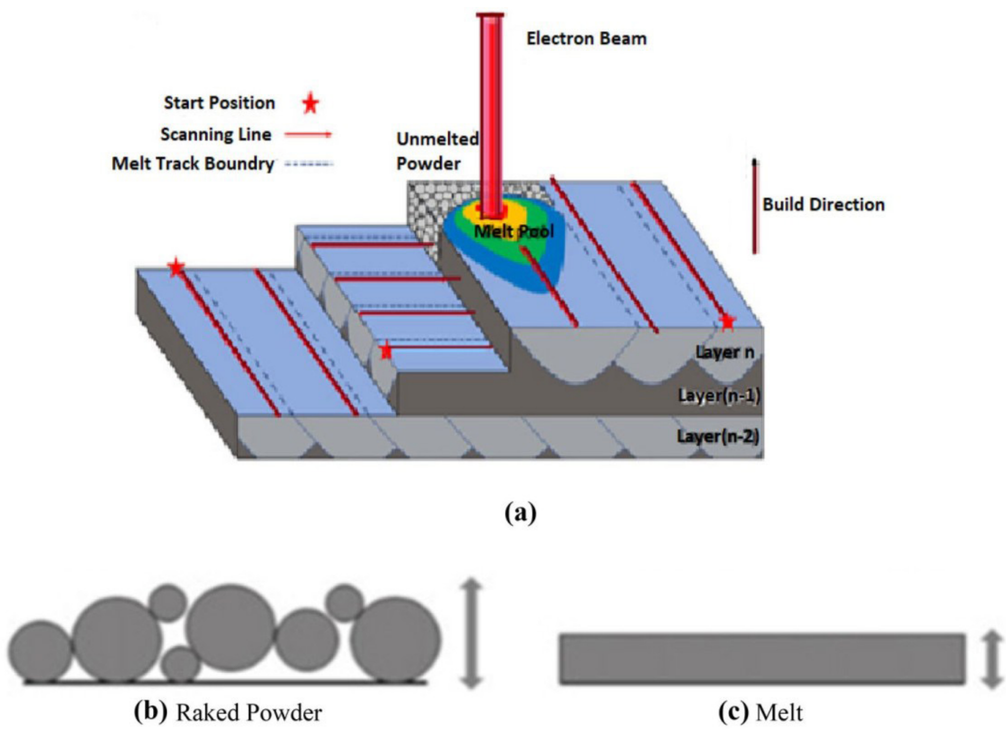

FIGURE 14. (a)EBT melting and raking system (b), (c) Powder layer thickness before & after (Amato et al. 2022; Murr 2019).

This advanced fabrication approach enables single-step production of intricate geometries including lattice frameworks and controlled-porosity structures. Medical implants with precisely engineered internal architecture can be manufactured to match specific anatomical requirements. The vacuum environment and elevated processing temperatures characteristic of this method minimize residual stress while maintaining exceptional process control (Figure 13). This technology's capacity to create metamaterials with auxetic properties structures with negative Poisson's ratios is one of its most notable features. Shear strength and fracture resistance are improved by such mechanical behaviour. Experimental studies have documented these ratios varying between 0.2 and 0.4, with significant orientation-dependent effects (Schwerdtfeger, Heinl, Singer, & Körner, 2020). Although its wider beam profile somewhat impairs precision, electron beam technology (EBT) greatly increases manufacturing efficiency by simultaneously heating multiple powder bed locations, in contrast to laser-based systems that process sequentially. Preheating also lowers the need for structural support. Typical EBT systems operate under high vacuum (10^-4 torr) using a tungsten filament electron source (50-60 kV) to process powders (45-105 µm particles) at remarkable scanning speeds (7000-8000 m/s) with ±0.025 mm accuracy across 0.05-0.2 mm layers (Amato et al. 2022) (Murr, 2019). The manufacturing sequence involves:

1. uniform powder distribution via raking system (Figure 14a),
2. preheating and selective melting (Figure 14b-c),
3. incremental platform lowering by one layer thickness, repeating until completion, followed by helium-assisted controlled cooling whose duration depends on material properties and component size.

This process enables rapid production while maintaining dimensional control, though with slightly reduced resolution compared to laser alternatives.

THE PROPERTIES OF MAGNESIUM ALLOYS IN TERMS OF THEIR MECHANICAL AND METALLURGICAL CHARACTERISTICS

Within the Mg-Al alloy system, AZ31 well-known of its outstanding properties, which considered as a dominant type of alloy, is widely utilized in both cast and wrought applications. However, research on laser-based (AM) of AZ31 remains scarce, with most studies focusing on wire-arc techniques instead. Laser-powder AM efforts have predominantly targeted higher-Al variants like AZ91, where aluminum enhances mechanical properties through solid-solution strengthening and Mg17Al12 precipitation, while also improving casting and printing performance. These high-Al alloys typically require grain refinement via superheating or inoculation. Despite the limited studies, Pawlak et. al. successfully demonstrated the laser powder bed fusion (LPBF) processing of AZ31, achieving exceptional density with porosity levels below 0.5% (Wei et al. 2019 – Influence of element vaporization on forma bility, composition, microstructure, and mechanical performance of theselective laser melted Mg–Zn–Zr components 2019). Similar results have been reported for AZ61 and AZ91 in LPBF, confirming the feasibility of processing Mg-Al alloys via this method. Microstructural analysis of laser powder bed fused AZ61 and AZ91 alloys reveals refined, equiaxed grain structures with minimal texture development, achieving grain diameters between 1-3 µm (Figure 15a). Previous investigations by research (C. He, 2020) (Wei et al. 2024), reported continuous networks of Mg17Al12 precipitates along grain boundaries, with clean grain interiors (Figure 15b).

On the other hand, our experimental data shows contradictory results: elongated grains parallel to the build direction (Figure 15c) with intragranular spherical nanoparticles (Figure 15d) and boundary precipitates (Figure 15c). These results were obtained using processing parameters of 50W laser power, 400 mm/s scan velocity, 40 µm hatch spacing, and 30 µm layer thickness, yielding an energy density of 104 J/mm^3. Notably, this energy input closely matches that reported by Jauer et. al. (Manakari, Parande, & Gupta) , despite their use of higher power (100W) and faster scanning (800 mm/s). The marked microstructural differences between these otherwise comparable cases suggest processing parameter adjustments can significantly alter grain morphology and precipitate distribution in Mg-Al alloys, though the underlying mechanisms require further investigation. These observations demonstrate the potential for microstructural engineering in LPBF-processed AZ-series alloys through precise control of fabrication conditions.

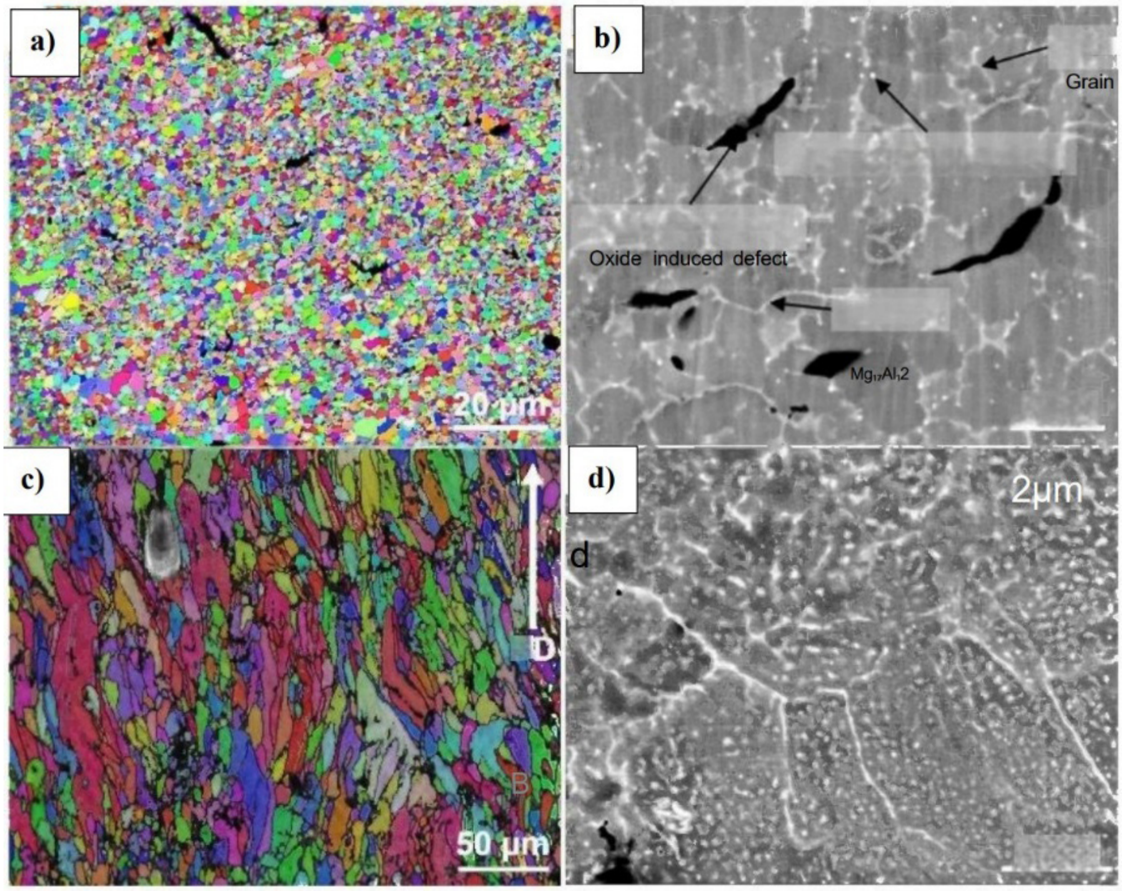

FIGURE 15. EBSD orientation map and SEM image of LPBF-AZ91 alloy (Wei et al. 2024)

In magnesium alloys containing 12.7 wt% aluminum, aluminum exhibits a high solubility. These magnesium-aluminum alloys are known for their excellent castability, moderate mechanical properties, and strong resistance to corrosion. The corrosion resistance of Mg-Al alloys can be significantly enhanced by increasing the aluminum content. To improve the strength and ductility at room temperature, zinc (Zn) or manganese (Mn) is often added to the aluminum matrix. Unlike aluminum, which can be harmful, zinc is an essential trace element for the human body. The yield strength steadily rises as the zinc concentration increases from 1 weight percent to 6 weight percent when zinc is added to magnesium. The proper zinc addition results in an elongation of 15.8% and an ideal ultimate tensile strength (UTS) of 216.8 MPa (Bamberger & Dehm, 2018; Wen, Wu, Dai, & Yang, 2021; Zhang, et al., 2020). The different mechanical properties of the magnesium alloy are presented in Table 1. The performance characteristics of engineered materials - including tensile strength, elastic modulus, ductility, and fatigue resistance - dictate their suitability for specific applications. Because of its mechanical compatibility with bone tissue, magnesium shows special potential for use in biomedical applications. Selective laser melting (SLM) magnesium alloys have elastic moduli (20.8-38.2 GPa) that nearly resemble those of natural bone (3-20 GPa). Research indicates these mechanical properties are strongly influenced by processing conditions, particularly laser energy density and powder characteristics. As illustrated in Figure 16, elevated energy densities promote grain coarsening in SLM-processed magnesium, which reduces the solute capture effect and consequently decreases material hardness. This relationship stems from the fundamental metallurgical principle that faster cooling rates produce finer grains through increased undercooling. Process parameters directly affect these cooling dynamics - reduced scan speeds combined with higher laser power (resulting in greater energy density) prolong melt pool duration, slowing heat dissipation and enabling grain growth.

Microstructural evolution in SLM magnesium alloys follows a predictable sequence with increasing energy input: from fine dendritic structures to uniform equiaxed grains, and obviously to coarse equiaxed formations (Liang et al. 2021). The well-established Hall-Petch relationship explains the resulting mechanical behavior, where refined grain structures (typically 1-15 µm in SLM magnesium) yield superior hardness compared to conventional processing methods. This grain refinement effect varies spatially within melt pools, with central regions exhibiting greater hardness than peripheral zones (Zhang & Zhang 2020) (Taltavull et al. 2022). The rapid solidification inherent to SLM processing enhances alloying element solubility in the magnesium matrix through the solute capture mechanism. This phenomenon significantly increases the incorporation of aluminum and zinc in the α-Mg phase, providing substantial solid solution strengthening. Nonetheless, by solute trapping, high energy inputs above ideal levels negate this positive impact, which in turn lowers hardness through a decrease in alloying element retention.

The dispersion of intermetallic compounds significantly influences microhardness in selective laser melted (SLM) magnesium alloys, as their non-uniform distribution alters dislocation dynamics and grain boundary interactions (Manakari et al. 2021). In Mg-Al systems, the β-$Mg_{17}Al_{12}$ phase (average hardness: ~174 Hv) exhibits greater hardness compared to the α-Mg matrix (~123 Hv), enhancing resistance to plastic deformation. Process-induced imperfections such as residual porosity, oxide inclusions, and thermal stresses further degrade mechanical properties, though strategic control of thermal gradients during fabrication can mitigate these defects and improve hardness (Taltavull et al. 2022). SLM-processed components demonstrate comparable or superior yield strengths relative to conventionally manufactured counterparts, attributed to rapid solidification rates that refine grain structures (1–15 µm vs. 200–300 µm in cast variants) and enhance compositional homogeneity. However, reduced ductility in SLM parts is often caused by incomplete fusing and microcracks, which are linked to less-than-ideal parameter selection. Experimental analyses show that tensile properties are inversely affected by changes in energy density. Reduced intermetallic phase formation and solute retention are linked to poorer ultimate tensile strength (286→254 MPa) and yield strength (274→237 MPa) in AZ91D alloys when input energy is reduced from 166.7 to 83.3 J/mm³ (Wei et al. 2024). Laser parameters critically oversee microstructural evolution. Elevated scan speeds or reduced power settings accelerate thermal dissipation, restricting grain growth and amplifying solute trapping effects—factors that enhance strength but risk incomplete powder fusion. This balance underscores the importance of optimizing energy density to maximize alloying element solubility while minimizing defects. Despite progress, further research is needed to systematically map processing windows for magnesium alloys, particularly in addressing the trade-offs between grain refinement, defect suppression, and mechanical performance (Long et al. 2020).

TABLE 1. Properties for Mg alloys (Jayasathyakawin et al. 2020)

Parent materials	Tensile strength (MPa)	Methods
ZK60/SiC	200	Powder processing
AZ61 AZXE7113	220	Powder processing
ZK61	236	Powder processing
WE43-B	220	Casting
AZ31–300C	202	Hot extrusion
6WE	220	Powder processing
AZ31	233	Twill roll casting
UST ZX	285	Solidification processing
UST ZX	456	Powder processing
Mg-1Al-0.3	246	Powder processing

Figure16 illustrates the microhardness of porous Mg-Zn-Zr alloys produced by powder bed fusion (PBF). The microhardness values of these alloys exhibited an exponential increase with rising zinc weight percentage. For the E1 alloy, the average microhardness was measured at 57.67 HV for the cross-section and 58.28 HV for the longitudinal section. The E2 alloy showed microhardness values of 75.51 HV and 80.23 HV for the cross-section and longitudinal section, respectively. On the other hand, the longitudinal and cross-sectional microhardness values of the E3 alloy were 109.36 and 106.75 HV, respectively. The PBF Mg-Zn-Zr alloys exhibit a discernible refinement of the grain structure as the zinc concentration rises. Grain refining can greatly increase the microhardness of magnesium alloys, according to the Hall-Petch relationship. Additionally, the Mg7Zn3 phase becomes more prevalent and coarser with increased zinc content. The presence of a uniformly distributed Mg7Zn3 phase is thought to impede dislocation movement between grains, contributing to the observed increase in microhardness (Zhang et al. 2021).

Figure 17 presents the microhardness measurements for the samples both prior to and following laser processing. The Mg–0.6Ca alloy exhibited a microhardness of 46±1 HV. Following to the laser treatment, the hardness of this alloy increased by 20%, reaching 56±1 HV. Similarly, the microhardness of the Mg–0.5Zn–0.3Ca alloy improved from 47±3 HV to 55±3 HV after laser processing, reflecting a 17% increase in hardness (Yao et al. 2021).

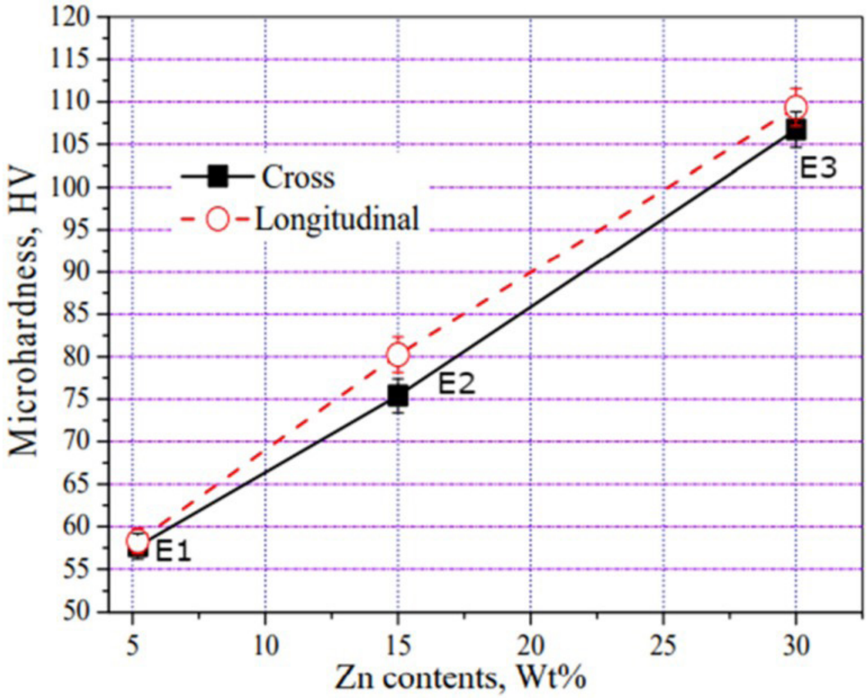

FIGURE 16. Microhardness of PBF alloys (Zhang et al. 2021)

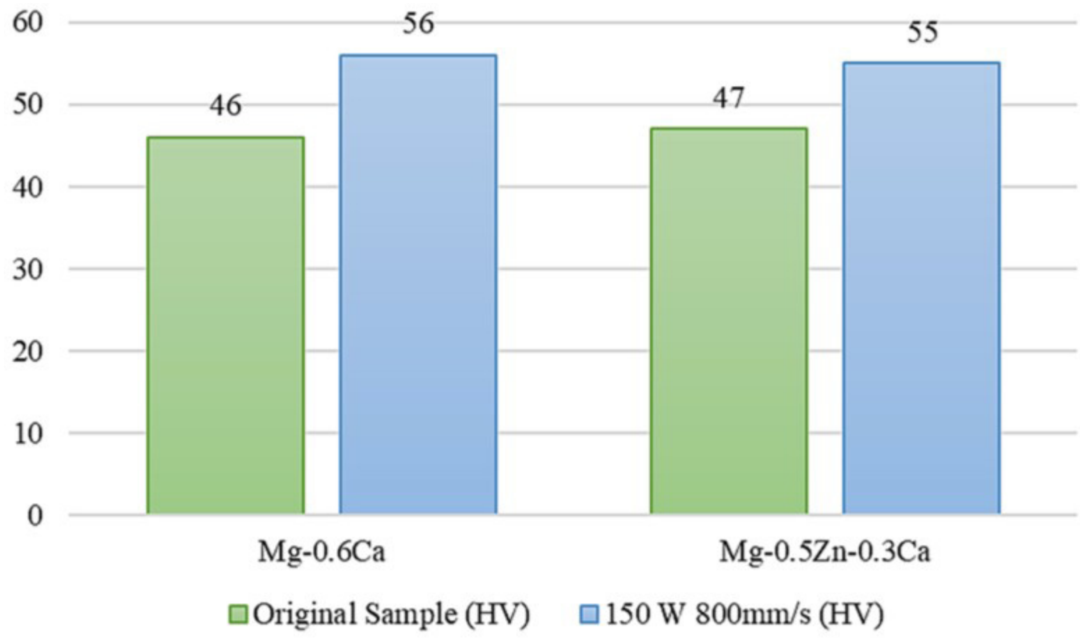

FIGURE 17. Microhardness of SLM samples (Yao et al. 2021)

CHALLENGES ASSOCIATED WITH THE PROCESSING OF MAGNESIUM ALLOYS

In its pure form, magnesium oxidizes rapidly, therefore it needs to be kept avoiding oxygen exposure. There are several types of raw materials accessible for additive manufacturing (AM), such as wires, liquid resins, and powders. In this state, the surface energy of magnesium increases, heightening the risk of combustion due to reactions with atmospheric oxygen. Additionally, there is a lack of comprehensive studies into the manufacturing processes for magnesium as a potential biodegradable alloy. To effectively print magnesium in an inert atmosphere while ensuring safe handling, specialized equipment is required. Therefore, the additive manufacturing of magnesium-based implants presents specific challenges due to the inherent properties of magnesium alloys, which include higher vapor pressure and increased reactivity (Wang et al. 2020; Tayier et al. 2020).

CONCLUSION

Magnesium has emerged as a highly promising material for the development of biomedical implants due to its superior biocompatibility and biodegradability. The ability to create customized magnesium components tailored to individual patient anatomies makes (AM) techniques particularly advantageous, especially for producing complex geometries. This review emphasizes the advantages of the powder bed fusion (plasma-based) process over other AM techniques to produce magnesium-based implants. Additionally, it discusses the different difficulties that arise during the manufacturing of magnesium implants and investigates possible ways to improve their qualities by using particular alloying elements and surface treatment methods. Bed fusion is identified as an effective AM technology for magnesium implants, as it facilitates efficient melting and infiltration of magnesium alloys, thereby minimizing voids and achieving high-density components. Furthermore, fusion or plasma-based processing's quick cooling rates and solidification produced better microstructural features like a more even phase distribution and finer grain structure. Compared to traditionally fabricated components, those produced via plasma-based processing exhibit better mechanical and corrosion resistance. Furthermore, both the parameters of the printing process and the properties of the powder significantly influence the biological and mechanical performance of the resulting magnesium scaffolds and implants.

ACKNOWLEDGEMENT

This research was supported in part by the from grant number: SEGiIRF/2022-Q1/FoEBEIT/001.

DECLARATION OF COMPETING INTEREST

None.

REFERENCES

Akhoundi, B., Behravesh, A. H. & Bagheri Saed, A. 2020. An innovative design approach in three-dimensional printing of continuous fiber-reinforced thermoplastic composites via fused deposition modeling process: In-melt simultaneous impregnation. *Proceedings of the Institution of Mechanical Engineers, Part B: Journal of Engineering Manufacture* 234(1–2): 243–259.

Amato, K. N., Gaytan, S. M., Murr, L. E., Martinez, E., Shindo, P. W., Hernandez, J. & Medina, F. J. A. M. 2022. Microstructures and mechanical behavior of Inconel 718 fabricated by selective laser melting. *Acta Materialia* 60(5): 2229–2239.

Babuska, T. F., Krick, B. A., Susan, D. F. & Kustas, A. B. 2021. Comparison of powder bed fusion and directed energy deposition for tailoring mechanical properties of traditionally brittle alloys. *Manufacturing Letters* 28: 30–34.

Bamberger, M. & Dehm, G. 2018. Trends in the development of new Mg alloys. *Annual Review of Materials Research* 38: 505–533.

Bose, S., Darsell, J., Kintner, M., Hosick, H. & Bandyopadhyay, A. 2023. Pore size and pore volume effects on alumina and TCP ceramic scaffolds. *Materials Science and Engineering: C* 23(4): 479–486.

Bose, S., Darsell, J., Kintner, M., Hosick, H. & Bandyopadhyay, A. 2021. Pore size and pore volume effects on alumina and TCP ceramic scaffolds. *Materials Science and Engineering: C* 23(4): 479–486.

Chen, X., Wang, X., Huan, P., Hu, Z., Wu, Z., Zhang, B. & Nagaumi, H. 2023. Effect of cold metal transfer mix synchro-pulse process on the overall morphology, microstructure and mechanical properties of wire arc additively manufactured AA2219 alloy. *Metals and Materials International* 29(2): 552–563.

Cho, H. W., Shin, S. J., Seo, G. J., Kim, D. B. & Lee, D. H. 2022. Real-time anomaly detection using convolutional neural network in wire arc additive manufacturing: Molybdenum material. *Journal of*

Materials Processing Technology 302: 117495.

DebRoy, T., Wei, H. L., Zuback, J. S., Mukherjee, T., Elmer, J. W., Milewski, J. O. & Zhang, W. 2020. Additive manufacturing of metallic components: Process, structure and properties. *Progress in Materials Science* 92: 112–224.

Denlinger, E. R., Heigel, J. C., Michaleris, P. & Palmer, T. A. 2020. Effect of inter-layer dwell time on distortion and residual stress in additive manufacturing of titanium and nickel alloys. *Journal of Materials Processing Technology* 215: 123–131.

Ding, J., Colegrove, P., Martina, F., Williams, S., Wiktorowicz, R. & Palt, M. R. 2019. Development of a laminar flow local shielding device for wire arc additive manufacture. *Journal of Materials Processing Technology* 226: 99–105.

Edwards, P., O'Conner, A. & Ramulu, M. 2022. Electron beam additive manufacturing of titanium components: Properties and performance. *Journal of Manufacturing Science and Engineering* 135(6): 061016.

Eivani, A. R., Mehdizade, M., Chabok, S. & Zhou, J. 2021. Applying multi-pass friction stir processing to refine the microstructure and enhance the strength, ductility and corrosion resistance of WE43 magnesium alloy. *Journal of Materials Research and Technology* 12: 1946–1957.

Fang, Z. C., Wu, Z. L., Huang, C. G. & Wu, C. W. 2020. Review on residual stress in selective laser melting additive manufacturing of alloy parts. *Optics & Laser Technology* 129: 106283.

Fang, X., Yang, J., Wang, S., Wang, C., Huang, K., Li, H. & Lu, B. 2022. Additive manufacturing of high performance AZ31 magnesium alloy with full equiaxed grains: Microstructure, mechanical property, and electromechanical corrosion performance. *Journal of Materials Processing Technology* 300: 117430.

Guo, Y., Pan, H., Ren, L. & Quan, G. 2020. Microstructure and mechanical properties of wire arc additively manufactured AZ80M magnesium alloy. *Materials Letters* 247: 4–6.

Guo, J., Zhou, Y., Liu, C., Wu, Q., Chen, X. & Lu, J. 2021. Wire arc additive manufacturing of AZ31 magnesium alloy: Grain refinement by adjusting pulse frequency. *Materials* 9(10): 823.

He, C., Bin, S., Wu, P., Gao, C., Feng, P., Yang, Y. & Shuai, C. 2020. Microstructure evolution and biodegradation behavior of laser rapid solidified Mg–Al–Zn alloy. *Metals* 7(3): 105.

Hafley, R. A. & Taminger, K. 2023. *Electron Beam Freeform Fabrication: A Rapid Metal Deposition Process*.

Herzog, D., Seyda, V., Wycisk, E. & Emmelmann, C. 2020. Additive manufacturing of metals. *Acta Materialia* 117: 371–392.

Horgar, A., Fostervoll, H., Nyhus, B., Ren, X., Eriksson, M. & Akselsen, O. M. 2020. Additive manufacturing using WAAM with AA5183 wire. *Journal of Materials Processing Technology* 259: 68–74.

Jayasathyakawin, S., Ravichandran, M., Baskar, N., Chairman, C. A. & Balasundaram, R. 2020. Mechanical properties and applications of magnesium alloy: Review. *Materials Today: Proceedings* 27: 909–913.

Jia, C., Liu, W., Chen, M., Guo, M., Wu, S. & Wu, C. 2020. Investigation on arc plasma, droplet, and molten pool behaviours in compulsively constricted WAAM. *Additive Manufacturing* 34: 101235.

Jiang, B., Xiang, Q., Atrens, A., Song, J. & Pan, F. 2021. Influence of crystallographic texture and grain size on the corrosion behaviour of as-extruded Mg alloy AZ31 sheets. *Corrosion Science* 126: 374–380.

Jiang, B., Xiang, Q., Atrens, A., Song, J. & Pan, F. 2022. Influence of crystallographic texture and grain size on the corrosion behaviour of as-extruded Mg alloy AZ31 sheets. *Corrosion Science* 126: 374–380.

Janasekaran, S. & Mann, S. 2020. A case study: Implementation of automated guided vehicle replacing trollies transportation in manufacturing industry to reduce motion waste in lean manufacturing practicing factory. *Journal of Engineering & Technological Advances* 5: 1–7.

Kopp, A., Derra, T., Müther, M., Jauer, L., Schleifenbaum, J. H., Voshage, M. & Kröger, N. 2020. Influence of design and postprocessing parameters on the degradation behavior and mechanical properties of additively manufactured magnesium scaffolds. *Acta Biomaterialia* 98: 23–35.

Karunakaran, R., Ortgies, S., Tamayol, A., Bobaru, F. & Sealy, M. P. 2020. Additive manufacturing of magnesium alloys. *Bioactive Materials* 5(1): 44–54.

Klein, T., Arnoldt, A., Schnall, M. & Gneiger, S. 2021. Microstructure formation and mechanical properties of a wire-arc additive manufactured magnesium alloy. *JOM* 73(4): 1126–1134.

Li, K., Ji, C., Bai, S., Jiang, B. & Pan, F. 2023. Selective laser melting of magnesium alloys: Necessity, formability, performance, optimization and applications. *Journal of Materials Science & Technology* 154: 65–93.

Liang, G., Ali, Y., You, G. & Zhang, M. X. 2021. Effect of cooling rate on grain refinement of cast aluminium alloys. *Materialia* 3: 113–121.

Long, T., Zhang, X., Huang, Q., Liu, L., Liu, Y., Ren, J. & Wu, H. 2020. Novel Mg-based alloys by selective laser melting for biomedical applications: Microstructure evolution, microhardness and in vitro degradation behaviour. *Virtual and Physical Prototyping* 13(2): 71–81.

Madhuri, N., Jayakumar, V. & Sathishkumar, M. 2021. Recent developments and challenges accompanying with wire arc additive manufacturing of Mg alloys: A review. *Materials Today: Proceedings* 46: 8573–8577.

Manakari, V., Parande, G. & Gupta, M. 2020. Selective laser melting of magnesium and magnesium alloy powders: A review. *Metals* 7(1): 2.

Mazumder, J., Dutta, D., Kikuchi, N. & Ghosh, A. 2020. Closed loop direct metal deposition: Art to part. *Optics and Lasers in Engineering* 34(4–6): 397–414.

Moritz, T. & Maleksaeedi, S. 2021. Additive manufacturing of ceramic components. In *Additive Manufacturing*, 105–161. Butterworth-Heinemann.

Murr, L. E. 2019. Metallurgy of additive manufacturing: Examples from electron beam melting. *Additive Manufacturing* 5: 40–53.

Palanivel, S., Nelaturu, P., Glass, B. & Mishra, R. S. 2023. Friction stir additive manufacturing for high structural performance through microstructural control in an Mg based WE43 alloy. *Materials & Design* 65: 934–952.

Popov, V. V., Grilli, M. L., Koptyug, A., Jaworska, L., Katz-Demyanetz, A., Klobčar, D. & Goel, S. 2021. Powder bed fusion additive manufacturing using critical raw materials: A review. *Materials* 14(4): 909.

Price, S., Lydon, J., Cooper, K. & Chou, K. 2023. *Experimental Temperature Analysis of Powder-Based Electron Beam Additive Manufacturing*.

Qin, Y., Wen, P., Guo, H., Xia, D., Zheng, Y., Jauer, L. & Schleifenbaum, J. H. 2020. Additive manufacturing of biodegradable metals: Current research status and future perspectives. *Acta Biomaterialia* 98: 3–22.

Ralston, K. D. & Birbilis, N. 2019. Effect of grain size on corrosion: A review. *Corrosion* 66(7): 075005-1.

Rodrigues, T. A., Duarte, V., Miranda, R. M., Santos, T. G. & Oliveira, J. P. 2020. Current status and perspectives on wire and arc additive manufacturing (WAAM). *Materials* 12(7): 1121.

Rudnev, V., Loveless, D. & Cook, R. L. 2017. *Handbook of Induction Heating*. CRC Press.

Sahasrabudhe, H., Bose, S. & Bandyopadhyay, A. 2020. Laser-based additive manufacturing processes. In *Advances in Laser Materials Processing*, 507–539.

Satya Prasad, V. V., Baligidad, R. G. & Gokhale, A. A. 2020. Niobium and other high temperature refractory metals for aerospace applications. In *Aerospace Materials and Material Technologies: Volume 1: Aerospace Materials*, 267–288. Singapore: Springer Singapore.

Schmidt, M., Merklein, M., Bourell, D., Dimitrov, D., Hausotte, T., Wegener, K. & Levy, G. N. 2022. Laser based additive manufacturing in industry and academia. *CIRP Annals* 66(2): 561–583.

Schwerdtfeger, J., Heinl, P., Singer, R. F. & Körner, C. 2020. Auxetic cellular structures through selective electron-beam melting. *Physica Status Solidi (B)* 247(2): 269–272.

Semiatin, S. L. 2000. *Elements of Induction Heating: Design, Control, and Applications*. ASM International.

Shi, J., Li, F., Chen, S. & Zhao, Y. 2020. T-GMAW based novel multi-node trajectory planning for fabricating grid stiffened panels: An efficient production technology. *Journal of Cleaner Production* 238: 117919.

Shuai, C., Yang, Y., Wu, P., Lin, X., Liu, Y., Zhou, Y. & Peng, S. 2022. Laser rapid solidification improves corrosion behavior of Mg-Zn-Zr alloy. *Journal of Alloys and Compounds* 691: 961–969.

Smalcerz, A. & Przylucki, R. 2023. Impact of electromagnetic field upon temperature measurement of induction heated charges. *International Journal of Thermophysics* 34(4): 667–679.

Snead, L. L., Hoelzer, D. T., Rieth, M. & Nemith, A. A. 2021. Refractory alloys: Vanadium, niobium, molybdenum, tungsten. In *Structural Alloys for Nuclear Energy Applications*, 585–640. Elsevier.

Sola, A. & Nouri, A. 2019. Microstructural porosity in additive manufacturing: The formation and detection of pores in metal parts fabricated by powder bed fusion. *Journal of Advanced Manufacturing and Processing* 1(3): 10021.

Tayier, W., Janasekaran, S., Vijayasree, V. P. & Tai, V. C. 2023. Morphology and microstructure studies of the zincalume steel joints using metal inert gas (MIG) process. *AIP Conference Proceedings* 2847(1): 020012.

Tayier, W., Janasekaran, S. & Vijayasree, V. P. 2022. Evaluation of heat input and bead geometry of zincalume steel (G550) welded joint between metal inert gas (MIG) and laser beam welding (LBW). *Materials Today: Proceedings* 48: 895–904.

Taltavull, C., Torres, B., López, A. J., Rodrigo, P., Otero, E. & Rams, J. 2022. Selective laser surface melting of a magnesium-aluminium alloy. *Materials Letters* 85: 98–101.

Turner, B. N. & Gold, S. A. 2021. A review of melt extrusion additive manufacturing processes: II. Materials, dimensional accuracy, and surface roughness. *Rapid Prototyping Journal* 21(3): 250–261.

Udenni Gunathilake, T. M. S., Ching, Y. C., Ching, K. Y., Chuah, C. H. & Abdullah, L. C. 2021. Biomedical and microbiological applications of bio-based porous materials: A review. *Polymers* 9(5): 160.

Vishnuram, P., Ramachandiran, G., Sudhakar Babu, T. & Nastasi, B. 2021. Induction heating in domestic cooking and industrial melting applications: A systematic review on modelling, converter topologies and control schemes. *Energies* 14(20): 6634.

Wang, Y., Fu, P., Wang, N., Peng, L., Kang, B., Zeng, H. & Ding, W. 2020. Challenges and solutions for the additive manufacturing of biodegradable magnesium implants. *Engineering* 6(11): 1267–1275.

Wang, X., Wang, A. & Li, Y. 2020. Study on the deposition accuracy of omni-directional GTAW-based additive manufacturing. *Journal of Materials Processing Technology* 282: 116649.

Warlimont, H. & Martienssen, W. eds. 2020. *Springer Handbook of Materials Data*. Springer.

Wei, K., Gao, M., Wang, Z. & Zeng, X. 2024. Effect of energy input on formability, microstructure and mechanical properties of selective laser melted AZ91D magnesium alloy. *Materials Science and Engineering: A* 611: 212–222.

Wei, K., Wang, Z. & Zeng, X. 2019. Influence of element vaporization on formability, composition, microstructure, and mechanical performance of the selective laser melted Mg-Zn-Zr components. *Materials Letters* 156: 187–190.

Wen, Z., Wu, C., Dai, C. & Yang, F. 2021. Corrosion behaviors of Mg and its alloys with different Al contents in a modified simulated body fluid. *Journal of Alloys and Compounds* 488(1): 392–399.

Wu, B., Pan, Z., Ding, D., Cuiuri, D., Li, H., Xu, J. & Norrish, J. 2020. A review of the wire arc additive manufacturing of metals: Properties, defects and quality improvement. *Journal of Manufacturing Processes* 35: 127–139.

Xiong, J., Yin, Z. & Zhang, W. 2021. Closed-loop control of variable layer width for thin-walled parts in wire and arc additive manufacturing. *Journal of Materials Processing Technology* 233: 100–106.

Yang, Y., He, C., Yang, W., Qi, F., Xie, D., Shen, L. & Shuai, C. 2020. Mg bone implant: Features, developments and perspectives. *Materials & Design* 185: 108259.

Yao, X., Tang, J., Zhou, Y., Atrens, A., Dargusch, M. S., Wiese, B. & Yan, M. 2021. Surface modification of biomedical Mg-Ca and Mg-Zn-Ca alloys using selective laser melting: Corrosion behaviour, microhardness and biocompatibility. *Journal of Magnesium and Alloys* 9(6): 2155–2168.

Yook, S. W., Kim, H. E. & Koh, Y. H. 2019. Fabrication of porous titanium scaffolds with high compressive strength using camphene-based freeze casting. *Materials Letters* 63(17): 1502–1504.

Yue, H., Fu, P., Li, Z. & Peng, L. 2020. Tensile crack initiation behavior of cast Mg–3Nd–0.2Zn–0.5Zr magnesium alloy. *Materials Science and Engineering: A* 673: 458–466.

Zhang, X. L. & Zhang, Z. T. 2020. Influence of sub-rapid solidification on microstructure and mechanical properties of AZ61A magnesium alloy. *Transactions of Nonferrous Metals Society of China* 18: 86–90.

Zhang, M., Chen, C., Liu, C. & Wang, S. 2022. Study on porous Mg-Zn-Zr ZK61 alloys produced by laser additive manufacturing. *Metals* 8(8): 635.

Zhang, T., Shao, Y., Meng, G., Cui, Z. & Wang, F. 2021. Corrosion of hot extrusion AZ91 magnesium alloy: I. Relation between the microstructure and corrosion behavior. *Corrosion Science* 53(5): 1960–1968.

Zhang, S., Zhang, Y., Gao, M., Wang, F., Li, Q. & Zeng, X. 2020. Effects of milling thickness on wire deposition accuracy of hybrid additive/subtractive manufacturing. *Science and Technology of Welding and Joining* 24(5): 375–381.

Zhang, S., Zhang, X., Zhao, C., Li, J., Song, Y., Xie, C. & Bian, Y. 2020. Research on an Mg-Zn alloy as a degradable biomaterial. *Acta Biomaterialia* 6(2): 626–640.